

A Steerable, Multi-Scale Singularity Index

Gautam S. Muralidhar, *Student Member, IEEE*, Alan C. Bovik, *Fellow, IEEE*, and Mia K. Markey, *Senior Member, IEEE*

Abstract—We propose a new steerable, multi-scale ratio index for detecting impulse singularities in signals of arbitrary dimensionality. For example, it responds strongly to curvilinear masses (ridges) in images, but minimally to step discontinuities. The ratio index employs directional derivatives of gaussians, making it naturally steerable and scalable. Experiments on real images demonstrate the efficacy of the index for detecting multi-scale curvilinear structures. A software version of the index can be downloaded from: <http://live.ece.utexas.edu/research/SingularityIndex/SingularityIndex.zip>.

Index Terms—Singularities, impulses, singularity detection, curvilinear structures.

I. INTRODUCTION

Detection of singularities is important for finding thin, dense structures in signals of one or more dimensions. For example, locating curve-like singularities in images is important in applications such as the detection of blood vessels and cancers, filaments in images of biological specimens, and roads and river deltas in satellite images [1].

Many approaches have been proposed to detect and localize impulse (mass) singularities. Mallat and Hwang [2] approached singularity detection by characterizing the Lipschitz regularity of image wavelet transform modulus extrema across scales and showed that the Lipschitz exponent reveals where a signal varies smoothly, and where there are edges, or impulse singularities. Lindeberg [3], [4] and Steger [5] presented a general scale-space framework for detecting edges and ridges in images.

We have developed a new ratio index for the detection of impulse singularities in signals of arbitrary dimensionality. It is inspired by conditions put forth by Lindeberg [3], [4] and Steger [5], by Canny's approach to edge detection [6], and by an energy operator developed by Teager and Kaiser [7]. The index employs steerable directional derivatives of gaussians yielding a computationally efficient multi-scale framework. We show analytically and experimentally that the index responds strongly to impulse- or ridge-like curves in images, and minimally to edges.

II. PROPOSED SINGULARITY INDEX IN 1-D

We first define the new singularity index in 1-D and in multiple dimensions afterwards. Let $f(x)$, $x \in R$, and $f'(x)$ and $f''(x)$ denote first and second order derivatives, respectively. Then define the dimensionless ratio index

$$(\psi f)(x) = \frac{|f(x)f''(x)|}{C + |f'(x)|^2} \quad (1)$$

The authors are with The University of Texas at Austin, Texas, USA.
E-mail: gautam.s.muralidhar@gmail.com

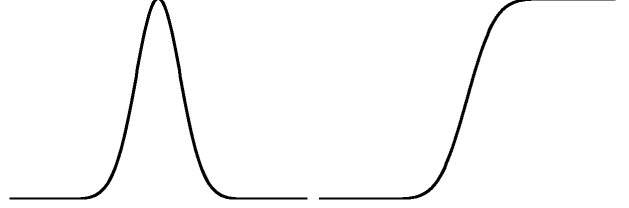


Fig. 1. 1-D impulse (left) and edge (right) profiles.

where $C \in R$. The index ψ responds strongly to impulse singularities, where the twice-derivative is large, but weakly to step singularities, where the once-derivative is large. Where the once-derivative is small, the denominator has little effect, suggesting the nominal value $C = 1$ although other criteria such as noise might promote other choices. For simplicity, assume $(\psi f)(x) = \frac{|f(x)f''(x)|}{1 + |f'(x)|^2}$.

To ensure invariance to local DC offset, the function $f(x)$ is locally debiased prior to computing $(\psi f)(x)$. This is done by everywhere subtracting the local mean computed using a large, unit area gaussian filter. The scale λ of this gaussian may be chosen as follows: consider a smoothed impulse of height K and scale w : $f(x) = Ke^{-\frac{x^2}{2w^2}}$ (Fig. 1, left). The locally debiased signal is $\hat{f}(x) = f(x) - g_\lambda(x) * f(x) = Ke^{-\frac{x^2}{2w^2}} - \frac{Kw}{\sqrt{\lambda^2 + w^2}} e^{-\frac{x^2}{2(\lambda^2 + w^2)}}$. At $x = 0$, $f(0) = K$, and $\hat{f}(0) = K - \frac{Kw}{\sqrt{\lambda^2 + w^2}}$. By choosing λ so that $|f(0) - \hat{f}(0)| \leq \epsilon K$, where $\epsilon \in (0, 1]$, the lower bound $\lambda \geq w\sqrt{\frac{1-\epsilon^2}{\epsilon^2}}$ is arrived at. Reasonable values of $w = 1.5$ and $\epsilon = 0.2$ yield $\lambda \geq 7.34$. We next analyze the behavior of the index on 1-D impulse and edge profiles.

A. 1-D Impulse Profile

Model a smoothed 1-D impulse as before by a gaussian of height $K > 0$ and scale w (see Fig. 1, left): $f(x) = Ke^{-\frac{x^2}{2w^2}}$. Then the index evaluates to

$$(\psi f)(x) = \frac{\left| \frac{K^2}{w^2} \left| \frac{x^2}{w^2} - 1 \right| e^{-\frac{x^2}{w^2}} \right|}{1 + \left| \frac{K^2}{w^4} \right| x^2 e^{-\frac{x^2}{w^2}}} \quad (2)$$

At $x = 0$, $(\psi f)(0) = \left| \frac{K^2}{w^2} \right|$. As $K \uparrow$, or $w \downarrow$, $(\psi f)(0) \uparrow$. The singularity index favors sharp impulses. As $w \rightarrow \infty$ or $x \rightarrow \infty$, then $\psi \rightarrow 0$. In the absence of other stimuli, the index vanishes with increased smoothness of, or distance from the impulse. It responds to both positive going and negative going impulses, although polarity is easily retained.

B. 1-D Edge Profile

Model a 1-D edge profile as a step $u(x)$ of height $K > 0$ smoothed by a gaussian $g_w(x)$ (see Fig. 1, right):

$$f(x) = Ku(x) * g_w(x) = K\Phi\left(\frac{x}{w}\right), \quad (3)$$

where $\Phi\left(\frac{x}{w}\right) = \frac{1}{\sqrt{2\pi}} \int_{-\infty}^{\frac{x}{w}} e^{-\frac{t^2}{2}} dt$. In this case, the singularity index evaluates to

$$(\psi f)(x) = \frac{\left(\left|\frac{K^2}{2\pi w^4}\right| |x| \left(\int_{-\infty}^x e^{-\frac{t^2}{2w^2}} dt\right) \left(e^{-\frac{x^2}{2w^2}}\right)\right)}{1 + \left(\left|\frac{K}{\sqrt{2\pi}w}\right|^2 e^{-\frac{x^2}{w^2}}\right)}. \quad (4)$$

At $x = 0$, the index vanishes: $(\psi f)(0) = 0$, and near the edge the index decreases with K .

C. Side-lobe Response

Lemma 1: For an impulse whose cross-section profile is a gaussian, the peak side-lobe response $(\psi f)_s$ of the singularity index is bounded by 1.

Proof: First notice that in (2), $(\psi f)(w) = 0$. The side-lobes occur at $|x| > w$. Let $A = \frac{K^2}{w^2}$ and $y = \frac{x^2}{w^2}$. Substituting these in (2) yields: $(\psi f)(y) = \frac{A|y-1|e^{-y}}{1+Ay e^{-y}}$.

Case 1: $y - 1 > 0 \Rightarrow (\psi f)(y) = \frac{A(y-1)e^{-y}}{1+Ay e^{-y}}$. Differentiating ψ w.r.t y and equating to 0 yields $(y-2)e^y = A$, the solution of which is the location of the peak side-lobe response. Substituting for A in ψ yields the peak side-lobe response $(\psi f)_s = \frac{y-2}{y-1} = \frac{x^2-2w^2}{x^2-w^2} \leq 1 \forall |x| > w$.

Case 2: $y - 1 < 0 \Rightarrow (\psi f)(y) = \frac{A(1-y)e^{-y}}{1+Ay e^{-y}}$. Differentiating ψ w.r.t y and equating to 0 again yields $(y-2)e^y = A$. Following similar (reversed) reasoning we find $|(\psi f)_s| \leq 1$.

From *Lemma 1*, $(\psi f)_s$ is bounded by 1 and does not depend on the impulse height K . By comparison, the simple impulse detector $f''(x)$ has a peak side-lobe response $\frac{0.446K}{w^2}$ at $x = \pm\sqrt{3}w$, which increases linearly with K for a fixed scale.

The singularity index does produce a small, but undesirable side-lobe response to edges. Rewrite (4) as $(\psi f)(z) = \frac{\left|\frac{K^2}{w^2}\Phi(z)\phi'(z)\right|}{1 + \frac{K^2}{w^2}\phi^2(z)}$, where $z = \frac{x}{w}$, $\phi(z) = \frac{1}{\sqrt{2\pi}}e^{-\frac{z^2}{2}}$ and $\Phi(z) = \int_{-\infty}^z \phi(t) dt$ are the standard normal probability density and cumulative distribution functions, respectively. Differentiating $(\psi f)(z)$ w.r.t z and equating to 0 yields a substitution for $\Phi(z)$, which when used in $(\psi f)(z)$ yields the peak edge side-lobe response $(\psi f)_{Es} = \frac{K^2 z^2 \phi^2(z)}{K^2(z^2+1)\phi^2(z) - w^2(z^2-1)}$. Unlike the impulse side-lobe response, the edge side-lobe response is not bounded by 1 and depends on K for a fixed scale w . However, the peak edge side-lobe response can be substantially attenuated as described next.

For some constant $a \in \mathbb{R}$, compute the first derivative response using a scale aw so that the singularity index becomes

$$(\psi f)(x) = \frac{|f(x)f'(x)|}{1 + |f'_a(x)|^2}. \quad (5)$$

To choose a , consider the edge model (3), where now $f'_a(x) = \frac{K}{aw}\phi\left(\frac{x}{aw}\right) = \frac{K}{\sqrt{2\pi}aw}e^{-\frac{x^2}{2a^2w^2}}$, and define $P(a) =$

$aw(f'_a(x))^2$. The optimal value for a is then taken to be $a^* = \operatorname{argmax}_a P(a) = \frac{\sqrt{2}x_0}{w}$, where x_0 is the location where the numerator $|ff'|$ is maximized in response to the step edge. Numerical solution yields $x_0 = 1.2554w$ and $a^* = 1.7754$. Extensive simulations using $a = 1.7754$ suggest that the peak side-lobe edge response of the singularity index computed with $f'_a(x)$ in (5) is upper bounded by 3.7. By comparison, $f''(x)$ has a peak side-lobe edge response $\frac{K}{\sqrt{2\pi}ew^2}$ at $x = \pm w$, which increases linearly with K for a fixed scale w .

D. Generalized Singularity Index

It is possible to control the scale of the singularity index by smoothing the signal first:

$$(\psi f)(x, \sigma) = \frac{|g_\sigma * f(x)| |g''_\sigma * f(x)|}{1 + |g''_{a\sigma} * f(x)|^2}, \quad (6)$$

where, g is a smoothing filter such as an unit-area gaussian: $g_\sigma(x) = \frac{1}{\sqrt{2\pi}\sigma}e^{-\frac{x^2}{2\sigma^2}}$. The first derivative of the smoothed signal is computed at a scale $a\sigma$ to attenuate the edge side-lobe responses. The use of gaussian filters stabilizes derivative computations and reduces noise. The concept of the index (6) can be generalized to detect other types of discontinuities such as edges. The k^{th} -order index

$$(\psi^k f)(x, \sigma) = \frac{|g_\sigma^{k-1} * f(x)| |g_\sigma^{k+1} * f(x)|}{1 + |g''_{a\sigma} * f(x)|^2} \quad (7)$$

includes (6) as a special case ($k = 1$). Odd integer values of k yield impulse detectors, while even integer values of k yield edge detectors.

E. Multi scale analysis

The smoothed singularity index (6) is easily extended to detect impulses at multiple scales. Consider a smoothed gaussian impulse of height $K > 0$ and scale w , i.e. $f(x) = Ke^{-\frac{x^2}{2w^2}}$. Then $f(x) * g_\sigma(x)$ is also gaussian: $f(x) * g_\sigma(x) = \frac{Kw}{\sqrt{\sigma^2+w^2}}e^{-\frac{x^2}{2(\sigma^2+w^2)}}$. Similarly, it can be shown that the first derivative response is $(f(x) * g_{a\sigma}(x))' = \frac{-Kwx}{((a\sigma)^2+w^2)^{3/2}}e^{-\frac{x^2}{2((a\sigma)^2+w^2)}}$ and the second derivative response is $(f(x) * g_\sigma(x))'' = \frac{-Kw}{(\sigma^2+w^2)^{3/2}} \left(\frac{-x^2 e^{-\frac{x^2}{2(\sigma^2+w^2)}}}{(w^2+\sigma^2)} + e^{-\frac{x^2}{2(\sigma^2+w^2)}} \right)$. Then $(\psi f)(0, \sigma) = \left| \frac{-K^2 w^2}{(\sigma^2+w^2)^2} \right| = \frac{K^2 w^2}{(\sigma^2+w^2)^2}$.

Now consider the scale normalized index $(\psi_{norm} f)(x, \sigma) = \sigma^{2\gamma}(\psi f)(x, \sigma)$, where $\gamma \in \mathbb{R}$. The scale-normalized index is motivated by the scale-space selection methodology based on local extrema over scales of γ -normalized derivatives that was proposed by Lindeberg in [4]. Then $(\psi_{norm} f)(0, \sigma)$ is maximized when $\sigma = \sqrt{\frac{2\gamma}{4-2\gamma}}w$, which matches the smoothed impulse width when $\gamma = 1$. Hence, the scale normalized index $(\psi_{norm} f)(x, \sigma) = \sigma^2(\psi f)(x, \sigma)$ attains a scale-space maxima at $\sigma = w$. Substituting this into the scale-normalized index yields $(\psi_{norm} f)(0, w) = \frac{K^2}{4}$, a constant independent of w . Thus, the scale-normalized singularity index is scale-invariant.

It is worth comparing the scale-normalized index to Lindeberg's γ -normalized *maximum eigenvalue of the Hessian* ridge strength measure, $M_{\gamma-norm}L$, defined in equation (46) in [3] for a smoothed gaussian impulse $f(x) = Ke^{\frac{-x^2}{2w^2}}$. As shown in [3], in order that the maximizing scale equal the width of the impulse, $\gamma = 3/4$. Substituting this into $M_{\gamma-norm}L$ yields a response of $\frac{K}{2^{3/2}\sqrt{w}}$ at the origin, which is not scale invariant.

III. PROPOSED SINGULARITY INDEX IN 2-D

The smoothed singularity index (6) is easily extended to detect curvilinear masses in 2-D. In 2-D, curvilinear masses are characterized by a dominant orientation. Hence, the sensitivity of the index can be improved by adopting a design mechanism inspired by Canny for edge detection [6]. First, determine the direction θ at each pixel along which the second derivative of the gaussian filtered image attains a local extremum, which is a good estimate of the direction orthogonal to a curvilinear mass. Once this direction is estimated, evaluate the responses of the gaussian derivative filters along this direction and compute the ratio index as follows:

$$(\psi f)(x, y, \sigma) = \frac{|f_{0,\theta,\sigma}(x, y)f_{2,\theta,\sigma}(x, y)|}{1 + |f_{1,\theta,a\sigma}(x, y)|^2} \quad (8)$$

In (8), $f_{0,\theta,\sigma}(x, y)$, $f_{1,\theta,a\sigma}(x, y)$, and $f_{2,\theta,\sigma}(x, y)$ are the responses to the zero, first and second order gaussian derivative filters along the direction specified by $\theta(x, y)$ and at scale σ . To estimate $\theta(x, y)$, deploy an isotropic gaussian filter and exploit the steerable property of gaussian directional derivatives as described in [8].

A. Multi-scale Realization

As in the 1-D case, the use of gaussian derivatives allows for an easy extension of the singularity index (8) to detect curvilinear masses at multiple scales. We employ a discrete, coarse-to-fine approach where (8) is computed in the order of decreasing scale σ . Automatic scale selection is achieved by selecting the scale yielding the largest scale normalized index value.

IV. EXPERIMENTS AND RESULTS

In all our experiments, we computed the scale-normalized singularity index i.e. $\sigma^2(\psi f)(x, y, \sigma)$. We fixed the lowest scale σ of the isotropic gaussian to 1.5 pixels, and the constant $a = 1.7754$. Each subsequent coarser scale was larger than the previous finer scale by a factor of $\sqrt{2}$. The number of scales was set to 6. Prior to computing the singularity index (8), the image was locally mean debiased using a large unit-volume isotropic gaussian with $\lambda \geq w\sqrt{\frac{1-\epsilon^2}{2}}$ pixels, where $\epsilon = 0.2$, and w was the largest scale. For comparison, we also show results using the scale normalized second derivative index i.e. $\sigma^{1.5}f_{2,\theta,\sigma}(x, y)$ and Lindeberg's *square of the γ -normalized eigenvalue difference* ridge strength measure ($A_{\gamma-norm}L$ in equation (51) in [3]). For $A_{\gamma-norm}L$, we used an implementation by Kokkinos *et al.* [9]. It has to be noted that $\sigma^{1.5}f_{2,\theta,\sigma}(x, y)$ exactly corresponds to the ridge strength measure $M_{\gamma-norm}L$ defined by Lindeberg in equation (46) in [3].

The scale normalized second derivative index was computed using the same set of scales as the singularity index, while Lindeberg's $A_{\gamma-norm}L$ measure [3] was computed using the same set of scales as the singularity index and also with a more exhaustive 50 scales (provided as the default setting in the implementation [9]). Further, the implementation provided by [9] applies a square-root transformation to $A_{\gamma-norm}L$ to yield a contour saliency measure whose dimensionality is the same as $\sigma^{1.5}f_{2,\theta,\sigma}(x, y)$. No such transformation is applied to the singularity index since it is dimensionless under the assumption that the constant in the denominator has a dimension *intensity*²/*length*².

Fig. 2 illustrates the results of the singularity index in rows 2 and 3, the scale normalized second derivative measure in rows 4 and 5, and Lindeberg's $A_{\gamma-norm}L$ measure (after the square-root transformation) in rows 6 and 7 on four images containing curvilinear structures - an aerial image (courtesy University of Southern California) in column 1, the Ganges river delta (NASA, courtesy of nasaimages.org) acquired as part of the NASA Human Spaceflight collection in column 2, a volcano on venus (NASA, courtesy of apod.nasa.gov) captured by the Magellan spacecraft in column 3, and an image of pine tree trunks in column 4. Each result illustrates the maximum response computed across all scales at every pixel location. The results in rows 3, 5, 6 and 7 are obtained after applying non-maxima suppression (NMS) along the dominant orientation at each pixel after the maximum response across all scales has been computed. For $\sigma^2(\psi f)(x, y, \sigma)$ and $\sigma^{1.5}f_{2,\theta,\sigma}(x, y)$, we use the steerability of gaussian derivatives to estimate the dominant orientation $\theta(x, y)$, while for $A_{\gamma-norm}L$, [9] uses the eigen directions of the Hessian matrix of the brightness function to estimate $\theta(x, y)$.

The results in Fig. 2 illustrate a strong response by the proposed singularity index to impulse-like structures, with suppressed response to edges. The normalized second derivative index (rows 4 and 5) produces significant response to edges as noted by Lindeberg too [3]. Lindeberg's $A_{\gamma-norm}L$ ridge strength measure (rows 6 and 7) produces a better response than the normalized second derivative index, but misses out on fine-scale impulses and lacks the contour continuity produced by the new singularity index (rows 2 and 3). A broader set of results on a total of 18 high-resolution images can be downloaded from: <http://live.ece.utexas.edu/research/SingularityIndex/SingularityIndex.zip>.

V. CONCLUSION AND FUTURE WORK

We presented a new steerable, multi-scale singularity index for analyzing impulse singularities in images. Our analyses and experiments reveal promising behavior by the index for detecting impulse-like or ridge curvilinear structures in images. The index is scalable and efficient due to the steerable directional derivatives of isotropic gaussians. We will explore the index in (7) for detecting generalized discontinuities in future work.

ACKNOWLEDGMENT

This work was supported under NSF grant number IIS-1116656. We would like to thank Reviewer 1 for insightful

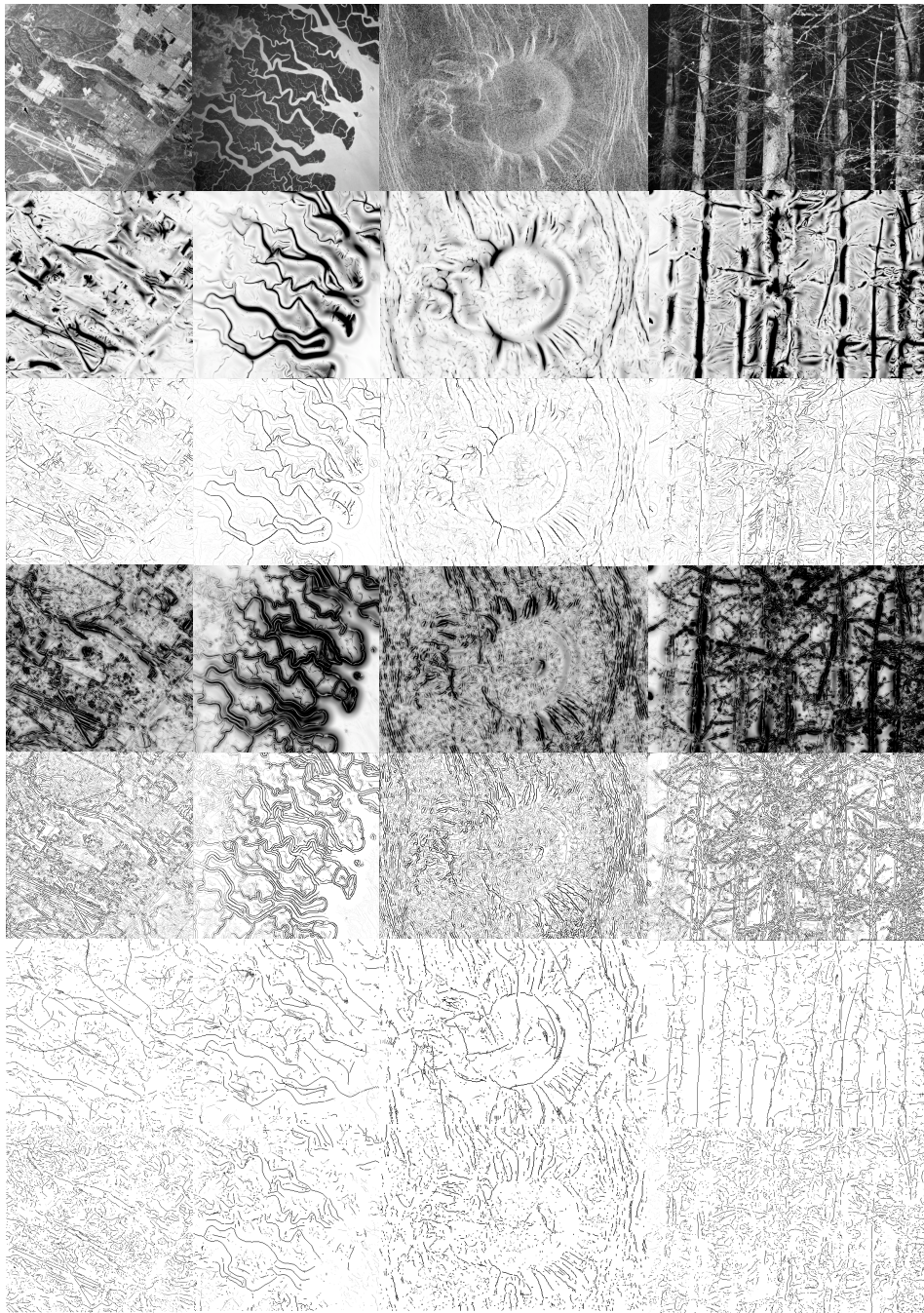


Fig. 2. Row 1: Original images; row 2: normalized singularity index result; row 3: NMS on singularity index result; row 4: normalized second derivative index; row 5: NMS on second derivative index; row 6: Lindeberg's $A_{\gamma-norm L}$ ridge strength measure using 50 scales; and row 7: Lindeberg's $A_{\gamma-norm L}$ ridge strength measure using 6 scales.

comments on our manuscript.

REFERENCES

- [1] T. M. Koller, G. Gerig, G. Szekely, and D. Dettwiler, "Multiscale detection of curvilinear structures in 2-d and 3-d image data," in *IEEE Intl. Conf. Comput. Vision*. IEEE, 1995, pp. 864–869.
- [2] S. Mallat and W. L. Hwang, "Singularity detection and processing with wavelets," *IEEE Trans. Inf. Theory*, vol. 38, no. 2, pp. 617–643, 1992.
- [3] T. Lindeberg, "Edge detection and ridge detection with automatic scale selection," *Intl. J. Comput. Vision*, vol. 30, no. 2, pp. 117–154, 1998.
- [4] —, "Feature detection with automatic scale selection," *Intl. J. Comput. Vision*, vol. 30, no. 2, pp. 77–116, 1998.
- [5] C. Steger, "An unbiased detector of curvilinear structures," *IEEE Trans. Pattern Anal. Mach. Intell.*, vol. 20, no. 2, pp. 113–125, 1998.
- [6] J. Canny, "A computational approach to edge detection," *IEEE Trans. Pattern Anal. Mach. Intell.*, vol. 8, no. 6, pp. 679–698, 1986.
- [7] J. F. Kaiser, "Some useful properties of teager's energy operators," in *IEEE Intl. Conf. Acoust., Speech, and Signal Process.*, vol. 3. IEEE, 1993, pp. 149–152.
- [8] W. T. Freeman and E. H. Adelson, "The design and use of steerable filters," *IEEE Trans. Pattern Anal. Mach. Intell.*, vol. 13, no. 9, pp. 891–906, 1991.
- [9] I. Kokkinos, P. Maragos, and A. Yuille, "Bottom-up and top-down object detection using primal sketch features and graphical models," in *IEEE Conf. Comput. Vision and Pattern Recog.* IEEE, 2006, pp. 1893–1900.